Communication

Quaternary Piperazine Substituted Rhodamines with Enhanced Brightness for Super-Resolution Imaging

Zhiwei Ye, Wei Yang, Chao Wang, Ying Zheng, Weijie Chi, Xiaogang Liu, Zhenlong Huang, Xiaoyuan Li, and Yi Xiao

J. Am. Chem. Soc., **Just Accepted Manuscript** • DOI: 10.1021/jacs.9b04893 • Publication Date (Web): 05 Sep 2019

Quaternary Piperazine Substituted Rhodamines with Enhanced Brightness for Super-Resolution Imaging

Zhiwei Ye[†,§], Wei Yang[†,‖,§,*], Chao Wang[‡,§], Ying Zheng[†,§], Weijie Chi[‡], Xiaogang Liu[‡,*], Zhenlong Huang[†], Xiaoyuan Li[†], and Yi Xiao[†,*]

[†] State Key Laboratory of Fine Chemicals, Dalian University of Technology, Dalian, 116024, China.

[‡] Singapore University of Technology and Design, 8 Somapah Road, Singapore 487372.

[‖] Chemical Analysis and Research Center, Dalian University of Technology, Dalian 116024, China

Supporting Information Placeholder

ABSTRACT: Insufficient brightness of fluorophores poses a major bottleneck for the advancement of super-resolution microscopes. Despite being widely used, many rhodamine dyes exhibit suboptimal brightness due to the formation of twisted intramolecular charge transfer (TICT) upon photoexcitation. Herein, we have developed a new class of quaternary piperazine substituted rhodamines with outstanding quantum yields (Φ = 0.93) and superior brightness (ε×Φ = 8.1 × 10^4 L·mol^{-1}·cm^{-1}), by utilizing the electronic inductive effect to prevent TICT. We have also successfully deployed these rhodamines in the super-resolution imaging of the microtubules of fixed cells, and cell membrane and lysosomes of live cells. Finally, we demonstrated that this strategy was generalizable to other families of fluorophores, resulting in substantially increased quantum yields.

Recent years have witnessed a rapid evolution of advanced fluorescence imaging techniques, such as single-molecule localization microscopy (SMLM)[1–3] that affords unprecedented resolution beyond the Abbe diffraction limit. In contrast to the rapid evolution of imaging techniques, the development of dyes with sufficient brightness and photostability remains slow, which poses a significant constraint to in-*vivo* cellular dynamic studies.[4,5] Therefore, it is urgent to develop bright and photostable dyes on the basis of rational molecular design strategies.

Rhodamines have been extensively utilized in many super-resolution imaging studies.[6–8] Ever since (probably) the first implementation of rhodamine spiroamide for SMLM in 2007,[9] photoswitchable rhodamines have been developed into versatile markers for localization-based super-resolution imaging of nucleus,[10–12] mitochondria,[10,13–16] endoplasmic reticulum,[14] tubulins,[16–18] actins,[19–22] lysosomes[19,23] and plasma membrane[24,25] in live or fixed cells.

Owing to these widespread applications, significant efforts have been taken to further enhance the performance of rhodamines.[26] Previous experimental studies have indicated some rhodamine's non-radiative decays match the formation of TICT states,[27–30] although other mechanisms, e.g., hydrogen-bonding interactions, could not be ruled out. Therefore, one of the important strategies in the development of new rhodamine derivatives is to suppress the probable TICT formation (Figure 1a).[31] In the TICT state, the donor moiety undergoes a ~90° rotation with respect to the fluorophore core, thus becoming non-radiative and highly reactive. To inhibit TICT, chemists used to rigidify dialkylamino donor moieties by forming ring structures. Unfortunately, this method often leads to large molecular structures with poor biological compatibility. Alternatively, Lavis *et al.*[11,13,32] replaced the *N,N*-dimethylamino substituent in tetramethylrhodamine (TMR) with an azetidine ring. Later, Xu and Liu *et al.*[33] further showed that an aziridine ring effectively suppresses TICT formation.

Herein, we employ a simple quaternary piperazine moiety to replace the dimethylamino group in TMR. The resulted N,N-dimethylpiperazine substituted rhodamine (MPR) doubles the brightness of TMR and maintains excellent biocompatibility.

Besides environmental conditions, TICT formation in a dye is intrinsically governed by two factors: steric hindrance (Lavis' and Xu's work) and electronic (or push-pull) effect (this work). We reason that reducing the electron-donating strength of the amino group would destabilize the TICT state and increase the energy barrier to enter the TICT state, thus suppressing TICT formation. This reasoning brings our attention to an electron-withdrawing quaternary piperazine moiety. Positively-charged ammonium exerts an inductive effect and reduces the electron donating capability of the adjacent amino group. Consequently, replacing the dimethylamino group with a quaternary piperazine moiety should minimize the TICT formation.

Our reasoning is supported by calculating vertical ionization energies (VIE) of a series of amino moieties

(Figure 1b). A large VIE corresponds to a weak electron-donating strength. Our results show that quaternary piperazine moieties have significantly larger VIE than other amino groups, indicating weak electron-donating strength.

We next computed the potential energy surface of TMR and MPR in water, as a function of the amino group rotation (Figures 1c, S1-S5). Our results show the TICT formation faces a considerably larger energy barrier in MPR (0.50 eV) than that in TMR (0.42 eV). Moreover, the driving energy to enter the TICT state from the local excited (LE) state in MPR (0.15 eV) is much less than that in TMR (0.60 eV). Therefore, TICT formation of MPR should be less likely than that of TMR.

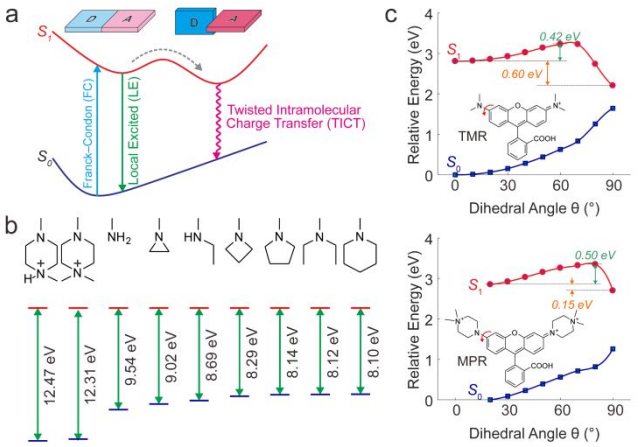

d

Core	Substituent (NR_1R_2)	Name	λ_{ab} [a] (nm)	λ_{em} [a] (nm)	Φ [a]	ε [a] ($\times 10^4$ $M^{-1}cm^{-1}$)
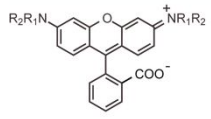		TMR	548	571	0.47	7.8[b]
		MPR	524	552	0.93	8.7
		Lyso-RH[c]	526	557	0.92	8.7
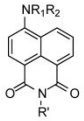		DM-Naph	441	554	0.009	0.98
		MP-Naph	388	528	0.71	0.96
		HP-Naph[c]	387	531	0.65	1.0
		DM-NBD	499	558	0.010 (0.017)[d]	3.6
		MP-NBD	469	539	0.087 (0.35)[d]	2.1
		HP-NBD[c]	472	543	0.086	2.1

[a] all photophysical properties were measured in MilliQ water of pH ≈ 7 unless stated otherwise; [b] Quoted from Ref. 11; [c] measured in pH = 4.0 aqueous solution; [d] measured in DMSO.

Figure 1. (a) Schematic illustrations of the potential energy profile, which leads to both emissive LE state and non-emissive TICT state. (b) Calculated vertical ionization energies of various amino groups in vacuo. (c) Calculated potential energy surfaces of TMR and MPR in water. (d) Spectroscopic properties of quaternary piperazine fluorophores and their dimethylamino analogs.

These theoretical calculations encouraged us to experimentally verify the quaternary piperazine strategy in enhancing the brightness of rhodamines. Therefore, we synthesized MPR through an effective *N*-alkylation to our previously reported piperazine rhodamine (SI Section 2.2).[34] Our spectroscopic studies demonstrate that MPR exhibited a significantly enhanced quantum yield (Φ = 0.93) and increased molar extinction coefficient (ε = 8.7 × 10^4 $M^{-1}cm^{-1}$) in aqueous solution, in comparison to TMR (Φ = 0.47; ε = 7.8 × 10^4 $M^{-1}cm^{-1}$). Similar enhancement was also found in Lyso-RH (Φ = 0.92, ε = 8.7 × 10^4 $M^{-1}cm^{-1}$), which is a protonated form of the piperazine rhodamine (Figure 1d; SI Section 3.3). Furthermore, in a systematical photophysical studies, the decreased non-radiative rates of TMR in less polar and viscous solvents indicate the probable existence of TICT states as well as other fluorescence quenching mechanisms (e.g., hydrogen-bonding),[35] while the near-unity quantum yield of Lyso-RH in water demonstrates that quaternary piperazine substitution suppresses this TICT state and most other nonradiative decays (SI Section 3.4). Overall, our strategy leads to more than one-fold increment in the ensemble brightness.

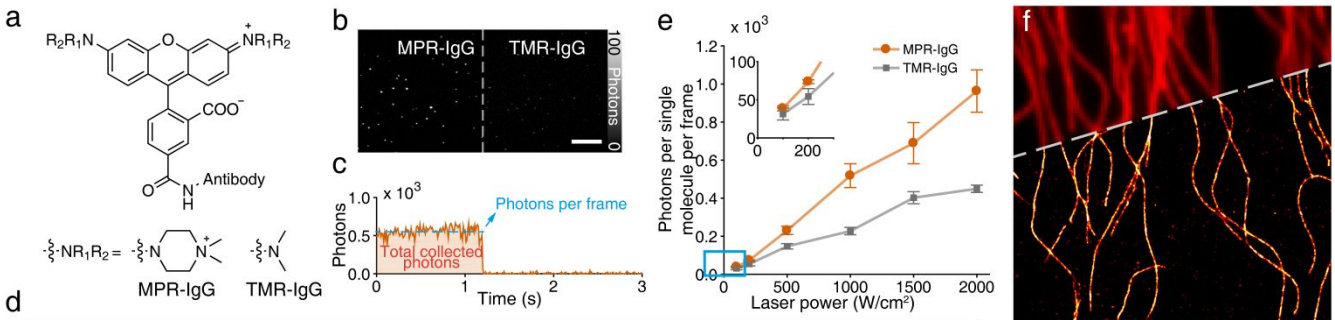

d

Dye	Brightness	Total collected photons (×10⁴)	Signal-to -noise ratio	Localization uncertainties (nm)	Condition
MPR-IgG	518±63	4.06±0.26	8.51±0.32	10.08±0.19	PBS
	1087±104	18.86±0.07	12.17±0.83	8.60±0.53	200 mM MEA
TMR-IgG	227±19	1.18±0.20	5.72±0.14	12.75±0.20	PBS
	470±46	6.67±0.95	7.59±0.40	11.43±0.25	200 mM MEA

Figure 2. (a) Carboxylic derivatives of MPR and TMR were coupled to IgG molecules. (b) Single-molecule fluorescent signals of MPR-IgG and TMR-IgG. (c) Single-molecule fluorescence trajectory of an MPR-IgG molecule. (d) Summary of single-molecule characteristics of MPR-IgG and TMR-IgG (n = 3). (e) Single-molecule brightness of MPR-IgG and TMR-IgG as a function of laser power in PBS (pH = 7.4) solution. (f) Super-resolution image of microtubules immunolabeled with a primary antibody against α-tubulin and MPR-IgG. A conventional image is overlaid on the upper side. Scale bars: 10 μm (b); 2 μm (f).

We further compared the fluorescence of MPR and TMR at the single-molecule level. Through carboxyl groups at the same position, both MPR (synthesis in SI Section 2.10) and TMR were coupled to immunoglobulin G (IgG; Figure 2a), and adsorbed on the surface of a coverslip, thus allowing the study of their single-molecule characteristics in aqueous conditions. As shown in Figure 2b, the single-molecule signals of both dyes are sparsely distributed, avoiding overlapping. A typical single-molecule fluorescence trajectory of MPR-IgG is depicted in Figure 2c, with the measurement of its single-molecule brightness (photons per single molecule per frame) and total collected photons before photobleaching. MPR-IgG demonstrates significant improvements of single-molecule brightness (518 ± 68), total collected photons (4.07 ± 0.26 × 10^4), signal-to-noise ratio (SNR: 8.51 ± 0.32) and localization precisions (10.08 ± 0.19 nm), compared to TMR-IgG (Figure 2d). These results match the ensemble spectroscopic studies as well as the quantum-chemical predictions. In addition, the enhanced photon statistics of MPR-IgG was confirmed at a series of conditions both in PBS and imaging enhancing buffer (Figure 2e; Table S4), and as indicated by a simulation study (Figure S18), MPR-IgG demonstrates an improved localization-based super-resolution imaging potential than TMR-IgG does (SI Section 4.5). Accordingly, these results demonstrate that quaternary piperazine strategy effectively enhanced the brightness of rhodamines.

To investigate utilities of the quaternary piperazine strategy in super-resolution imaging, we immunostained microtubules in HeLa cells. Reconstructed image (Figure 2f) reveals the twists and crosses of microtubules, exhibiting a considerable enhancement of clarity compared to a conventional image. Quantitative analysis of the reconstruction (Figure S21) estimated a 14.9 nm localization uncertainty and 96.3 nm FRC (Fourier ring correlation)[36,37] resolution. Moreover, the comparison of imaging results indicates an enhanced super-resolution imaging capability of MPR than that of TMR (Figures S22-24).

To further investigate MPR's applicability in live cells, we designed a bipolar probe, Mem-R (Φ = 0.64, Figure 3a; synthesis in SI Section 2.9), to specifically label plasma membranes. Indeed, confocal imaging confirms this specificity of Mem-R (Figure S19).

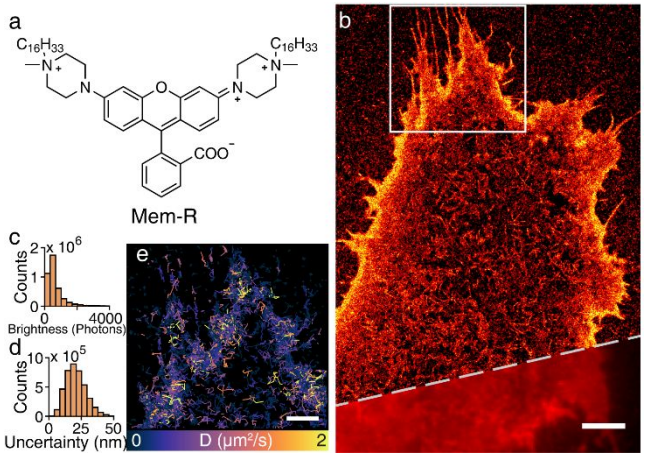

Figure 3. (a) Molecular structure of Mem-R. (b) Super-resolution image of the plasma membrane of a live HeLa cell stained with Mem-R. The bottom side is overlaid with a conventional image from the same region. Histogram of single-molecule brightness (c) and localization uncertainties (d) in (b). (e) High-density molecular tracking of Mem-R in the marked region in (b). Trajectories were colored according to their diffusion coefficients. Scale bars: 4 μm (b); 2 μm (e).

We then performed super-resolution imaging of cell membranes using Mem-R. Sufficiently sparse single-

molecule signals were collected, probably resulting from the exchangeable binding of Mem-R on the cell membrane (Movie S1; SI Section 6.4). The reconstruction image (Figures 3b, S25) reveals the detailed architecture of cell membrane in stark comparison with a blurred conventional image. Further analysis of the reconstruction estimated an average single-molecule brightness of 984 (Figure 3c) and an average localization precision of 20.9 nm (Figure 3d). We further compared its super-resolution imaging results of membrane with Mem-TMR (an analog membrane targetable probe based on TMR; synthesis in SI section 2.11). The results in Figures S26-27 indicate that Mem-R hold a significantly enhanced capability of super-resolution imaging than Mem-TMR. We noted that the single-molecule brightness of Mem-R was comparable to that of DiI (a Cy3 based commercial membrane tracker; Figure S28a), which should be ascribed to the much higher quantum yield of Mem-R than DiI in context of the much higher absorption coefficient of the latter probe (ε = 148 000 $M^{-1}cm^{-1}$)[38]. Moreover, as shown in Figure 3e, the excellent photophysical properties of Mem-R enable high-density single-molecule track experiment, which reveals a heterogeneous diffusion of Mem-R on the plasma membrane. These results show that Mem-R permits super-resolution imaging of cell membrane with high quality.

Recently, we have reported the lysosomal targetability of Lyso-R[34]. As shown in Figure 4a, the probe Lyso-R is mostly non-protonated and exhibit low fluorescence at neutral pH, whereas its protonation ($pk_{1/2}$ = 6.56; Figure S10) results in the formation of a highly fluorescent Lyso-RH, fulfilling our quaternary piperazine strategy. We hypothesized that this protonation induced bright-dark transformation and the diffusion equilibrium of the probe between cytosol and acidic organelles would develop a desirable photoswitching behavior beneficial for super-resolution imaging. To confirm the targetability of Lyso-RH, we performed a diffraction-limited confocal colocalization analysis with a lysosomal marker protein (Lamp-1) in live HeLa cells. Lyso-RH demonstrates a good affinity towards lysosomes (Pearson correlation coefficient: 0.84, *n* = 21; Figure S20).

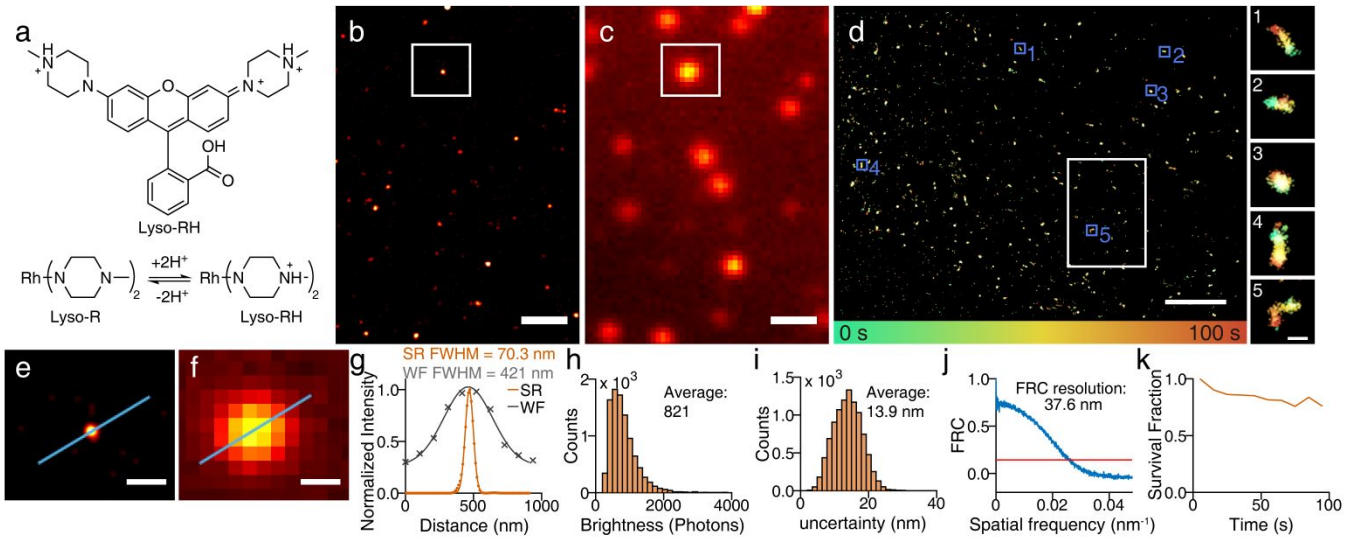

Figure 4. (a) Protonation of Lyso-R generates Lyso-RH in *situ* in acidic lysosomes. (b) Super-resolution and (c) conventional images of lysosomes in a live HeLa cell stained with Lyso-RH. (d) Time colored super-resolution images of lysosomes. The white box highlights the imaging region of (b). Magnified views of typical lysosomes are presented on the right. Images (e) and (f) were magnified views of the highlighted regions in (b) and (c). (g) Intensity distributions across the blue lines in (e) and (f). Histogram of single-molecule brightness (h) and localization uncertainties (i) in (b). (j) FRC analysis[37] of (b). (k) The survival fraction of molecules during imaging of (d). Scale bars: 4 μm (o); 1 μm (b, c); 300 nm (e,f); 200 nm (d 1-5).

We performed super-resolution imaging of lysosomes in live HeLa cells with Lyso-RH. Temporal separated signals repeatedly appeared in lysosomes of live cells under normal culture media, probably owing to the protonation equilibrium and the intracellular redox system[39] (Movie S2; SI Section 6.4). Statistical analysis showed that the brightness of photoswitching events of Lyso-RH (Figure S28b) surpasses that of the commercial Lysotracker Red. The reconstruction images revealed the true shape and size of globular lysosomes (Figure 4b, 4e) with significantly improved clarity than diffraction limited images (Figure 4c, 4f). The width of the lysosome is measured to be 70.3 nm in the super-resolution image, matching the reported values from electron microscopy,[40,41] whereas this width is estimated to be 421 nm in a conventional image (Figure 4g). Quantification analysis of the reconstruction demonstrates high spatial resolution (average localization precision: 13.9 nm, Figure 4i; overall resolution: 37.6 nm, Figure 4j), comparable with previously reported results (Table S5). Besides, owing to the durable photoswitching of Lyso-RH in lysosomes even without excessive imaging enhancing agents (Figure 4k), a long-term super-resolution imaging (Figure 4d) was achieved, showing heterogeneous movements of lysosomes with high spatial resolutions (Figure 4d 1-5).

Finally, we explored the generalizability of the quaternary piperazine strategy. Quantum-chemical calculations predicted that this strategy was translational to other fluorophores, such as naphthalimide and NBD dyes (Figures S6-S7) and subsequent experiments demonstrate an enhancement of brightness by up to 77 times (Figure 1d).

In conclusion, we have proposed and demonstrated a new strategy to enhance the brightness of rhodamine dyes by employing the quaternary piperazine as a donor fragment to reduce the push-pull effect and inhibit twisted intramolecular charge transfer. The newly designed MPR exhibited >1-fold improvement in brightness comparing to conventional TMR. Based on MPR, we further developed one cell-membrane probe Mem-R and one lysosome probe Lyso-RH. Their outstanding fluorescence properties enabled successful applications in single-molecule tracking and super-resolution imaging experiments.

We expect that the quaternization strategy will inspire the development of numerous high-performance fluorophores and probes, and greatly facilitate the development of fluorescent imaging techniques.

ASSOCIATED CONTENT

Supporting Information

The Supporting Information is available free of charge on the ACS Publications website.

Experimental methods, synthesis procedures, compound characterization, Figure S1-S53 and Table S1-S5. (PDF)

Movie S1. Single-molecule signals of Mem-R on the plasma membrane. (AVI)

Movie S2. Single-molecule signals of Lyso-RH in lysosomes. (AVI)

AUTHOR INFORMATION

Corresponding Author

xiaoyi@dlut.edu.cn; (Y. Xiao)
xiaogang_liu@sutd.edu.sg; (X. Liu)
yw917@dlut.edu.cn. (W. Yang)

Author Contributions

§These authors contributed equally.

Notes

The authors declare no competing financial interests.

ACKNOWLEDGMENT

This work is supported by National Natural Science Foundation of China (Nos. 21376038, 21421005, 21576040, 21776037 and 21804016), the Singapore University of Technology and Design (T1SRCI17126) and SUTD-MIT International Design Center (IDG31800104). The computational work is conducted with support from SUTD-MIT International Design Center and National Supercomputing Centre (NSCC) Singapore. The fluorescent imaging is performed with support from Chemical Analysis and Research Center, Dalian University of Technology.

REFERENCES

(1) Rust, M. J.; Bates, M.; Zhuang, X. Sub-Diffraction-Limit Imaging by Stochastic Optical Reconstruction Microscopy (STORM). *Nat. Methods* **2006**, *3*, 793–796.

(2) Betzig, E.; Patterson, G. H.; Sougrat, R.; Lindwasser, O. W.; Olenych, S.; Bonifacino, J. S.; Davidson, M. W.; Lippincott-Schwartz, J.; Hess, H. F. Imaging Intracellular Fluorescent Proteins at Nanometer Resolution. *Science* **2006**, *313* (5793), 1642–1645.

(3) Hess, S. T.; Girirajan, T. P. K.; Mason, M. D. Ultra-High Resolution Imaging by Fluorescence Photoactivation Localization Microscopy. *Biophys. J.* **2006**, *91* (11), 4258–4272.

(4) Liu, Z.; Lavis, L. D.; Betzig, E. Imaging Live-Cell Dynamics and Structure at the Single-Molecule Level. *Mol. Cell* **2015**, *58* (4), 644.

(5) van de Linde, S.; Heilemann, M.; Sauer, M. Live-Cell Super-Resolution Imaging with Synthetic Fluorophores. *Annu. Rev. Phys. Chem.* **2012**, *63* (1), 519–540.

(6) Lavis, L. D. Chemistry Is Dead. Long Live Chemistry! *Biochemistry* **2017**, *56*, 5165–5170.

(7) Butkevich, A. N.; Lukinavičius, G.; D'Este, E.; Hell, S. W. Cell-Permeant Large Stokes Shift Dyes for Transfection-Free Multicolor Nanoscopy. *J Am Chem Soc* **2017**, *139*, 12378–12381.

(8) Butkevich, A. N.; Bossi, M. L.; Lukinavičius, G.; Hell, S. W. Triarylmethane Fluorophores Resistant to Oxidative Photobluing. *J. Am. Chem. Soc.* **2019**, *141* (2), 981–989.

(9) Fölling, J.; Belov, V.; Kunetsky, R.; Medda, R.; Schönle, A.; Egner, A.; Eggeling, C.; Bossi, M.; Hell, S. W. Photochromic Rhodamines Provide Nanoscopy with Optical Sectioning. *Angew. Chem., Int. Ed.* **2007**, *46* (33), 6266–6270.

(10) Carlini, L.; Manley, S. Live Intracellular Super-Resolution Imaging Using Site-Specific Stains. *ACS Chem. Biol.* **2013**, *8* (12), 2643–2648.

(11) Grimm, J. B.; English, B. P.; Chen, J.; Slaughter, J. P.; Zhang, Z.; Revyakin, A.; Patel, R.; Macklin, J. J.; Normanno, D.; Singer, R. H.; Lionnet, T.; Lavis, L. D. A General Method to Improve Fluorophores for Live-Cell and Single-Molecule Microscopy. *Nat. Methods* **2015**, *12*, 244–250.

(12) Legant, W. R.; Shao, L.; Grimm, J. B.; Brown, T. A.; Milkie, D. E.; Avants, B. B.; Lavis, L. D.; Betzig, E. High-Density Three-Dimensional Localization Microscopy across Large Volumes. *Nat. Methods* **2016**, *13* (4), 359–365.

(13) Grimm, J. B.; English, B. P.; Choi, H.; Muthusamy, A. K.; Mehl, B. P.; Dong, P.; Brown, T. A.; Lippincott-Schwartz, J.; Liu, Z.; Lionnet, T.; Lavis, L. D. Bright Photoactivatable Fluorophores for Single-Molecule Imaging. *Nat. Methods* **2016**, *13*, 985–988.

(14) Takakura, H.; Zhang, Y.; Erdmann, R. S.; Thompson, A. D.; Lin, Y.; McNellis, B.; Rivera-Molina, F.; Uno, S.; Kamiya, M.; Urano, Y.; Rothman, J. E.; Bewersdorf, J.; Schepartz, A.; Toomre, D. Long Time-Lapse Nanoscopy with Spontaneously Blinking Membrane Probes. *Nat. Biotechnol.* **2017**, *35*, 773–780.

(15) He, H.; Ye, Z.; Xiao, Y.; Yang, W.; Qian, X.; Yang, Y. Super-Resolution Monitoring of Mitochondrial Dynamics upon Time-Gated Photo-Triggered Release of Nitric Oxide. *Anal. Chem.* **2018**, *90* (3), 2164–2169.

(16) Ye, Z.; Yu, H.; Yang, W.; Zheng, Y.; Li, N.; Bian, H.; Wang, Z.; Liu, Q.; Song, Y.; Zhang, M.; Xiao, Y. Strategy to Lengthen the On-Time of Photochromic Rhodamine Spirolactam for Super-Resolution Photoactivated Localization Microscopy. *J. Am. Chem. Soc.* **2019**, *141* (16), 6527–6536.

(17) Uno, S.; Kamiya, M.; Yoshihara, T.; Sugawara, K.; Okabe, K.; Tarhan, M. C.; Fujita, H.; Funatsu, T.; Okada, Y.; Tobita, S.; Urano, Y. A Spontaneously Blinking Fluorophore Based on Intramolecular Spirocyclization for Live-Cell Super-Resolution Imaging. *Nat. Chem.* **2014**, *6*, 681–689.

(18) Uno, S.; Kamiya, M.; Morozumi, A.; Urano, Y. A Green-Light-Emitting, Spontaneously Blinking Fluorophore Based on Intramolecular Spirocyclization for Dual-Colour Super-Resolution Imaging. *Chem. Commun.* **2018**, *54* (1), 102–105.

(19) Pan, D.; Hu, Z.; Qiu, F.; Huang, Z.-L.; Ma, Y.; Wang, Y.; Qin, L.; Zhang, Z.; Zeng, S.; Zhang, Y.-H. A General Strategy for Developing Cell-Permeable Photo-Modulatable Organic Fluorescent Probes for Live-Cell Super-Resolution Imaging. *Nat. Commun.* **2014**, *5*, 5573.

(20) Kiuchi, T.; Higuchi, M.; Takamura, A.; Maruoka, M.; Watanabe, N. Multitarget Super-Resolution Microscopy with High-Density Labeling by Exchangeable Probes. *Nat. Methods* **2015**, *12* (8), 743–746.

(21) Grimm, J. B.; Klein, T.; Kopek, B. G.; Shtengel, G.; Hess, H. F.; Sauer, M.; Lavis, L. D. Synthesis of a Far-Red Photoactivatable Silicon-Containing Rhodamine for Super-Resolution Microscopy. *Angew. Chem., Int. Ed.* **2016**, *128* (5), 1755–1759.

(22) Macdonald, P. J.; Gayda, S.; Haack, R. A.; Ruan, Q.; Himmelsbach, R. J.; Tetin, S. Y. Rhodamine-Derived Fluorescent Dye with Inherent Blinking Behavior for Super-Resolution Imaging. *Anal. Chem.* **2018**, *90* (15), 9165–9173.

(23) He, H.; Ye, Z.; Zheng, Y.; Xu, X.; Guo, C.; Xiao, Y.; Yang, W.; Qian, X.; Yang, Y. Super-Resolution Imaging of Lysosomes with a Nitroso-Caged Rhodamine. *Chem. Commun.* **2018**, *54* (23), 2842–2845.

(24) Takakura, H.; Zhang, Y.; Erdmann, R. S.; Thompson, A. D.; Lin, Y.; McNellis, B.; Rivera-Molina, F.; Uno, S.; Kamiya, M.; Urano, Y.; Rothman, J. E.; Bewersdorf, J.; Schepartz, A.; Toomre, D. Long Time-Lapse Nanoscopy with Spontaneously Blinking Membrane Probes. *Nat. Biotechnol.* **2017**, *35*, 773–780.

(25) Qi, Q.; Chi, W.; Li, Y.; Qiao, Q.; Chen, J.; Miao, L.; Zhang, Y.; Li, J.; Ji, W.; Xu, T.; Liu, X.; Yoon, J.; Xu, Z. A H-Bond Strategy to Develop Acid-Resistant Photoswitchable Rhodamine Spirolactams for Super-Resolution Single-Molecule Localization Microscopy. *Chem. Sci.* **2019**, *10* (18), 4914–4922.

(26) Mitronova, G. Y.; Belov, V. N.; Bossi, M. L.; Wurm, C. A.; Meyer, L.; Medda, R.; Moneron, G.; Bretschneider, S.; Eggeling, C.; Jakobs, S.; Hell, S. W. New Fluorinated Rhodamines for Optical Microscopy and Nanoscopy. *Chem. – A Eur. J.* **2010**, *16* (15), 4477–4488.

(27) Vogel, M.; Rettig, W.; Sens, R.; Drexhage, K. H. Structural Relaxation of Rhodamine Dyes with Different N-Substitution Patterns: A Study of Fluorescence Decay Times and Quantum Yields. *Chem. Phys. Lett.* **1988**, *147* (5), 452–460.

(28) Chang, T.-L.; Cheung, H. C. A Model for Molecules with Twisted Intramolecular Charge Transfer Characteristics: Solvent Polarity Effect on the Nonradiative Rates of Dyes in a Series of Water—Ethanol Mixed Solvents. *Chem. Phys. Lett.* **1990**, *173* (4), 343–348.

(29) Chang, T.; Borst, W. L. Effect of Solvent Polarity on a Rotational Isomerization Mechanism of Rhodamine-B in Normal Alcohols. *J. Chem. Phys.* **1990**, *93* (7), 4724–4729.

(30) Casey, K. G.; Quitevis, E. L. Effect of Solvent Polarity on Nonradiative Processes in Xanthene Dyes: Rhodamine B in Normal Alcohols. *J. Phys. Chem.* **1988**, *92* (23), 6590–6594.

(31) Grabowski, Z. R.; Rotkiewicz, K.; Rettig, W. Structural Changes Accompanying Intramolecular Electron Transfer: Focus on Twisted Intramolecular Charge-Transfer States and Structures. *Chem. Rev.* **2003**, *103* (10), 3899–4032.

(32) Grimm, J. B.; Muthusamy, A. K.; Liang, Y.; Brown, T. A.; Lemon, W. C.; Patel, R.; Lu, R.; Macklin, J. J.; Keller, P. J.; Ji, N.; Lavis, L. D. A General Method to Fine-Tune Fluorophores for Live-Cell and in Vivo Imaging. *Nat. Methods* **2017**, *14* (10), 987.

(33) Liu, X.; Qiao, Q.; Tian, W.; Liu, W.; Chen, J.; Lang, M. J.; Xu, Z. Aziridinyl Fluorophores Demonstrate Bright Fluorescence and Superior Photostability by Effectively Inhibiting Twisted Intramolecular Charge Transfer. *J. Am. Chem. Soc.* **2016**, *138* (22), 6960–6963.

(34) Ye, Z.; Xiao, Y.; Guo, H.; Wang, C. Specific and Photostable Rhodamine-Based Tracker for 3D Video Imaging of Single Acidic Organelles. *RSC Adv.* **2014**, *4* (71), 37547.

(35) Bassolino, G.; Nançoz, C.; Thiel, Z.; Bois, E.; Vauthey, E.; Rivera-Fuentes, P. Photolabile Coumarins with Improved Efficiency through Azetidinyl Substitution. *Chem. Sci.* **2018**.

(36) Banterle, N.; Bui, K. H.; Lemke, E. A.; Beck, M. Fourier Ring

Correlation as a Resolution Criterion for Super-Resolution Microscopy. *J. Struct. Biol.* **2013**, *183* (3), 363–367.

(37) Nieuwenhuizen, R. P. J.; Lidke, K. A.; Bates, M.; Puig, D. L.; Grünwald, D.; Stallinga, S.; Rieger, B. Measuring Image Resolution in Optical Nanoscopy. *Nat. Methods* **2013**, *10*, 557–562.

(38) *The Molecular Probes Handbook: A Guide to Fluorescent Probes and Labeling Technologies*; Spence, M. T. Z., Johnson, I. D., Eds.; Life Technologies Corporation, 2010.

(39) Schafer, F. Q.; Buettner, G. R. Redox Environment of the Cell as Viewed through the Redox State of the Glutathione Disulfide/Glutathione Couple. *Free Radic. Biol. Med.* **2001**, *30* (11), 1191–1212.

(40) Bright, N. A.; Gratian, M. J.; Luzio, J. P. Endocytic Delivery to Lysosomes Mediated by Concurrent Fusion and Kissing Events in Living Cells. *Curr. Biol.* **2005**, *15* (4), 360–365.

(41) Nishida, T.; Yoshimura, R.; Endo, Y. Three-Dimensional Distribution of TrkA Neurotrophin Receptors in Neurite Varicosities of Differentiated PC12 Cells Treated with NGF Determined by Immunoelectron Tomography. *Cell Tissue Res.* **2013**, *351* (1), 1–13.

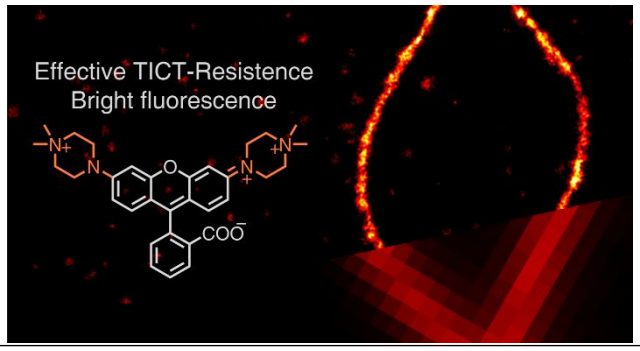
Effective TICT-Resistence
Bright fluorescence
COO⁻